Supporting Information

Direct mapping of local director field of nematic liquid crystals at the nanoscale

Yu Xia[a], Francesca Serra[a,b,c], Randall D. Kamien[b], Kathleen J. Stebe[c], and Shu Yang[a,*]

[a] Department of Materials Science and Engineering, University of Pennsylvania, 3231 Walnut Street, Philadelphia, PA 19104, USA
[b] Department of Physics and Astronomy, University of Pennsylvania, 209 South 33rd Street, Philadelphia, PA 19104, USA
[c] Department of Chemical and Biomolecular Engineering, University of Pennsylvania, Towne Building, 220 South 33rd Street, Philadelphia, PA 19104, USA

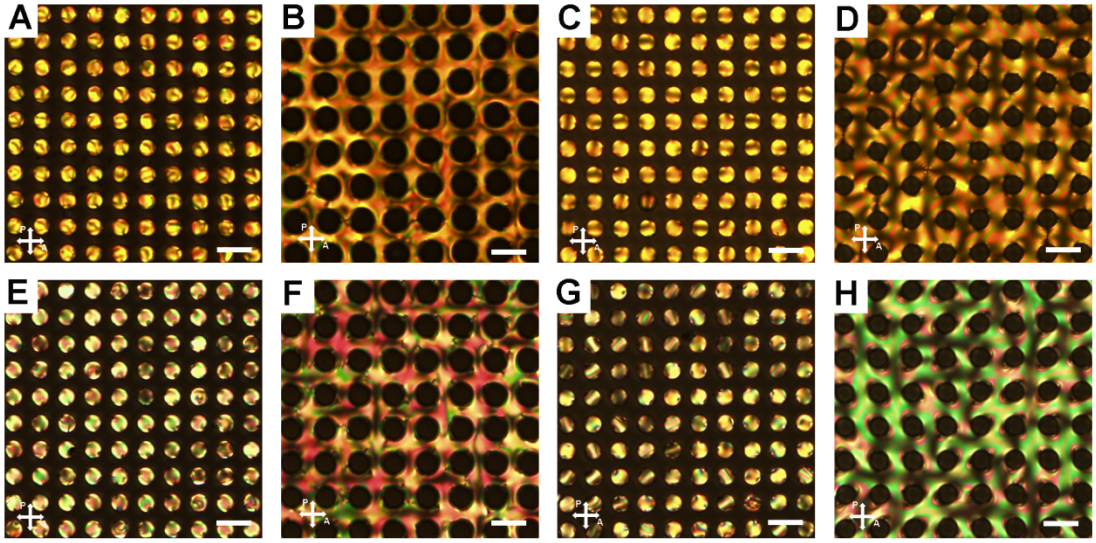

Fig. S1. POM images of LCM_AZO [4-ethoxy-4'-(6-acryloyloxyhexyloxy) azobenzene] and RM257 [(1,4-Bis-[4-(6-acryloyloxyhexyloxy)benzoyloxy]-2-methylbenzene)] on various patterned epoxy substrates coated with different surface chemistry. (A) LCM_AZO in polyvinyl alcohol (PVA) coated square array of pores. (B) LCM_AZO between PVA coated square array of pillars. (C) LCM_AZO in dimethyloctadecyl[3-(trimethoxysilyl)propyl]ammonium chloride (DMOAP) coated square array of pores. (D) LCM_AZO between DMOAP coated square array of pillars. (E) RM257 in PVA coated square array of pores. (F) RM257 between PVA coated square array of pillars. (G) RM257 in DMOAP coated square array of pores. (H) RM257 between DMOAP coated square array of pillars. Scale bar applied to all figures: 20 μm.

Pores in A, C, E, and G: diameter: 10 μm, pitch: 15 μm, depth: 20 μm.
Pillar arrays in B, D, F, and H: diameter: 10 μm, pitch: 20 μm, height: 19 μm.
Samples were cooled slowly (1 ^{o}C/min) from isotropic phase (100 ^{o}C for LCM_AZO and 130 ^{o}C for RM257) to nematic phase (94 ^{o}C for LCM_AZO and 125 ^{o}C for RM257).

Since the surface energy of the boundary determines the anchoring behavior of liquid crystal molecules (homeotropic or planar),[1] we prepared patterned surfaces with both high (PVA) and low (DMOAP) surface energy. However, as seen from Fig. S1, it is clear that both LCM_AZO and RM257 fail to align uniformly on patterned surfaces regardless of the surface energy of the coatings and surface geometry. They mostly show polydomains with disclination lines either in the bulk or pinned to the boundaries. Although this non-equilibrium alignment can be improved by carefully annealing the sample through the nematic-isotropic phase transition, it is non-trivial to achieve the ideal equilibrium state with monodomains.

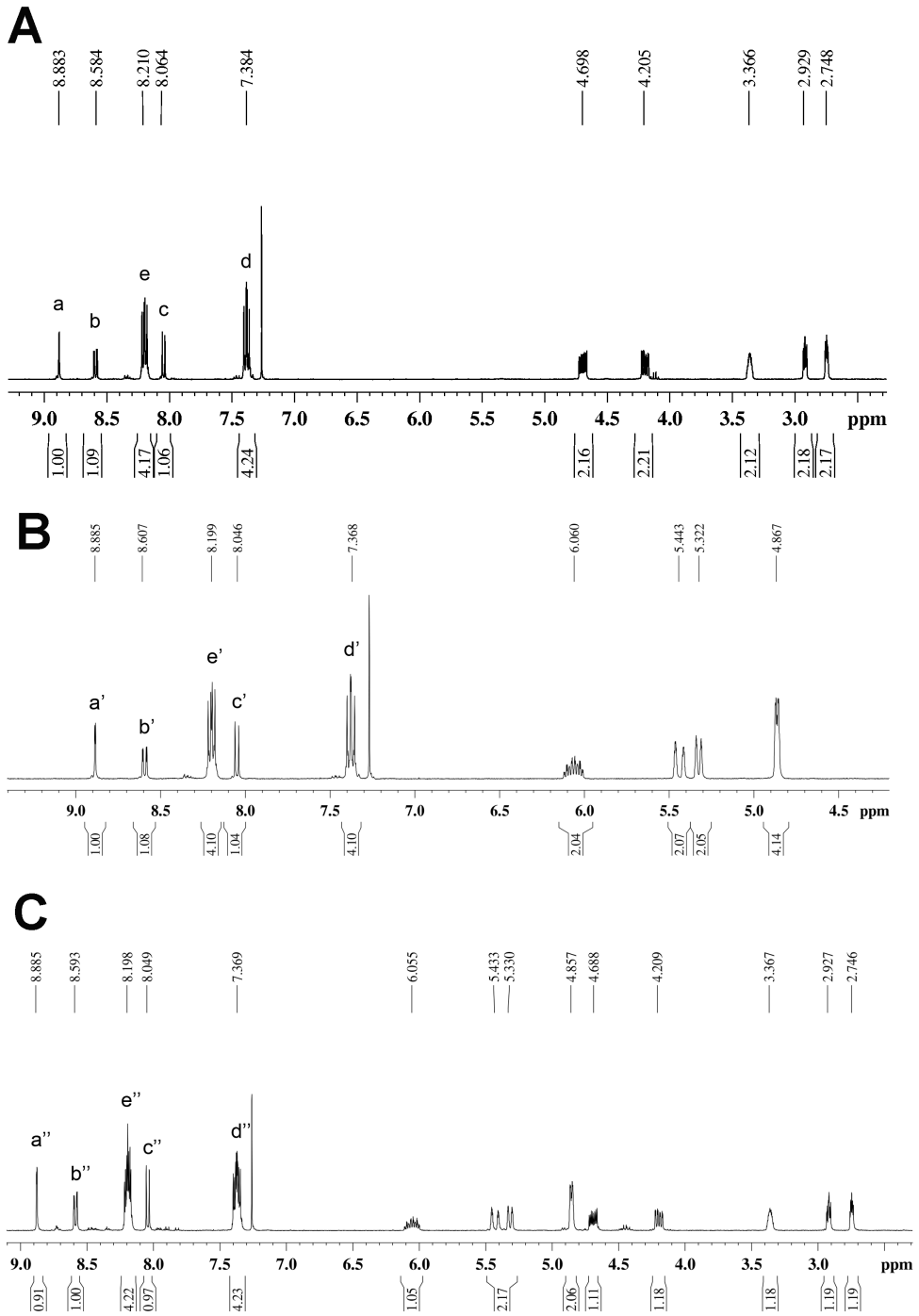

Fig. S2. [1]H-NMR spectrum of the liquid crystal monomers (A) LCM_X1; (B) LCM_X2; (C) LCM_X3. Chemical structure of each monomer can be found in the main text, Fig. 1, and the corresponding proton labels can be found in Fig. 2.

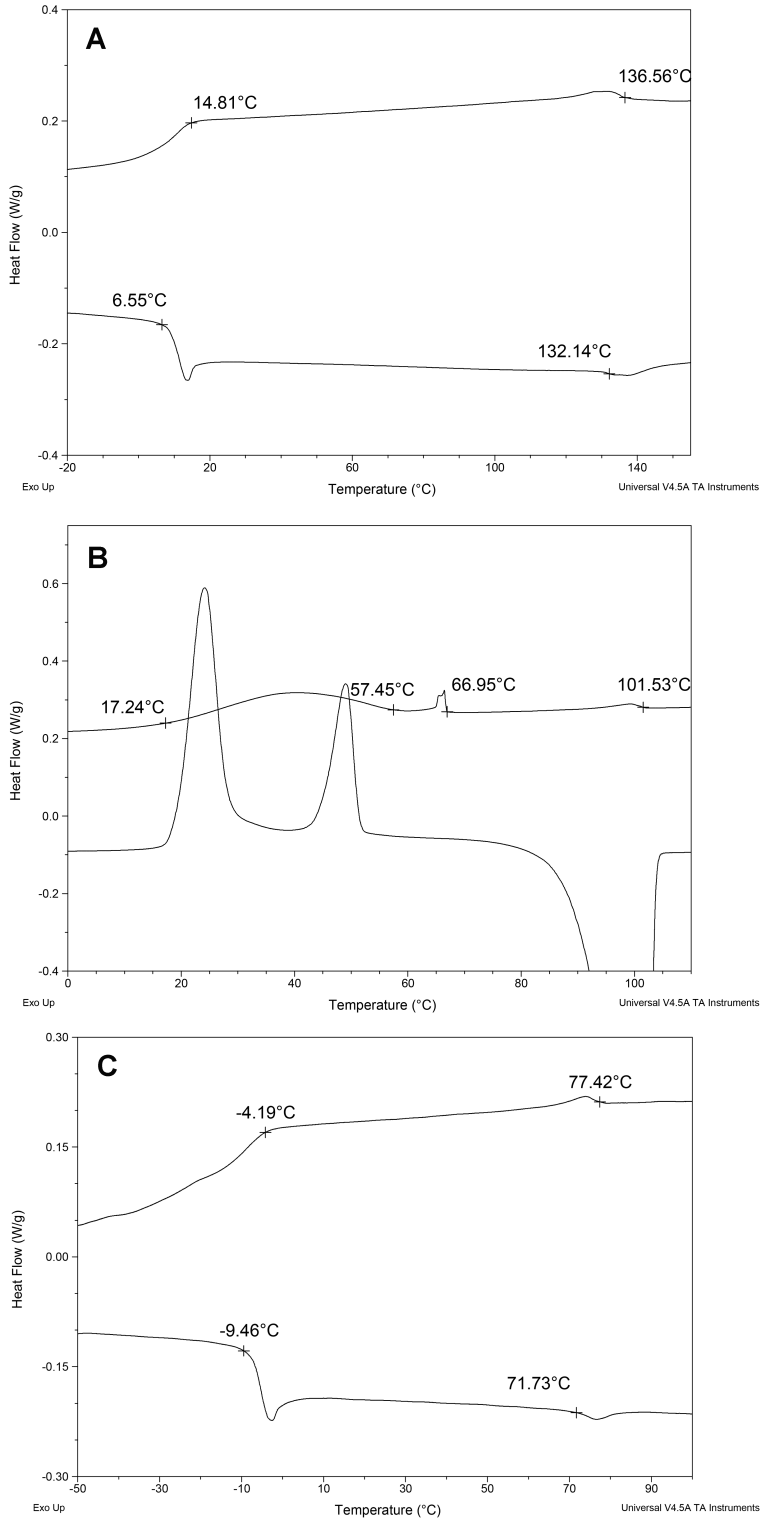

Fig. S3. DSC curves of the LCMs. (A) LCM_X1. A nematic phase from 6.5 ºC to 132 ºC (heating) and 136 ºC to 15 ºC (cooling), respectively, was observed. (B) LCM_X2. A nematic phase was only observed upon cooling from 101 ºC to 57 ºC*. (C) LCM_X3.

A nematic phase was shown from -9 ºC to 72 ºC (heating) and 77 ºC to -4 ºC (cooling), respectively.
*: A small peak at ~ 67 ºC was observed, which could be attributed to packing of the end alkene groups of LCM_X2, since the system was still in the nematic phase at 65 ºC as verified by POM.

DSC curves in Fig. S3 show that LCM_X1 and X3 did not crystalize upon cooling while LCM_X2 presented crystallization spreading over a large temperature range (~ 57 ºC to ~ 17 ºC). It is clear that the crystallization of all LCM's was suppressed since there are multiple bonding sites designed in our systems with strong intermolecular dipole interactions.

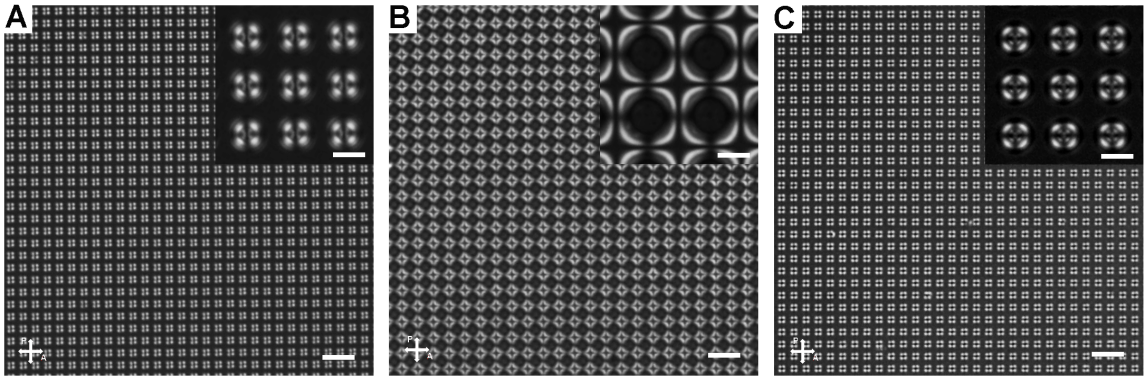

Fig. S4. POM images of various LCMs on patterned substrates with homeotropic anchoring at the boundaries. (A) LCM_X2 in the square array of pores. (B) LCM_X2 between the square array of pillars. (C) LCM_X3 in the square array of pores. Scale bars: 40μm. Insets: POM images with higher magnification. Scale bars: 10μm.

Pores in A&C: diameter: 10 μm, pitch: 15 μm, depth: 20 μm. Pillar arrays in (B): diameter: 10 μm, pitch: 20 μm, height: 19 μm. Samples were fast cooled (~20 ^{o}C/min) from isotropic phase (LCM_X2, 110 ^{o}C; LCM_X3, 85 ^{o}C) to nematic phase (LCM_X2, 90 ^{o}C; LCM_X3, 70 ^{o}C).

Fig. S4 clearly demonstrates that even without careful cooling, the samples achieved equilibrium quickly and formed organized anchoring configurations over the entire sample area.

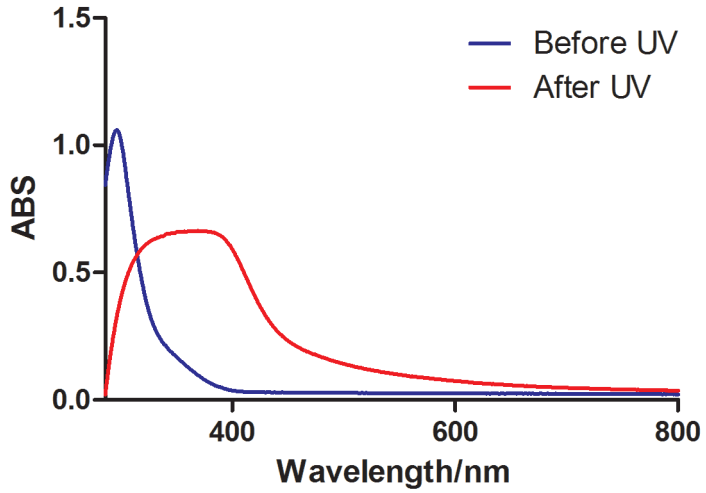

Fig. S5. UV-Vis spectra of LCM_X1 before and after UV curing.

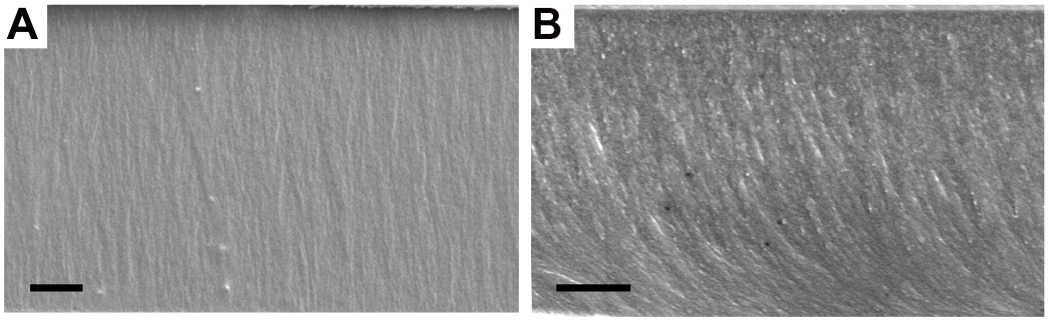

Fig. S6. SEM images of fracture structures of liquid crystal polymers (LCPs) in different LC cells. (A) A homeotropic cell. (B) A hybrid cell with homeotropic anchoring on the top, and uniform planar anchoring at the bottom (on a rubbed polyimide). Scale bars: 2 μm.

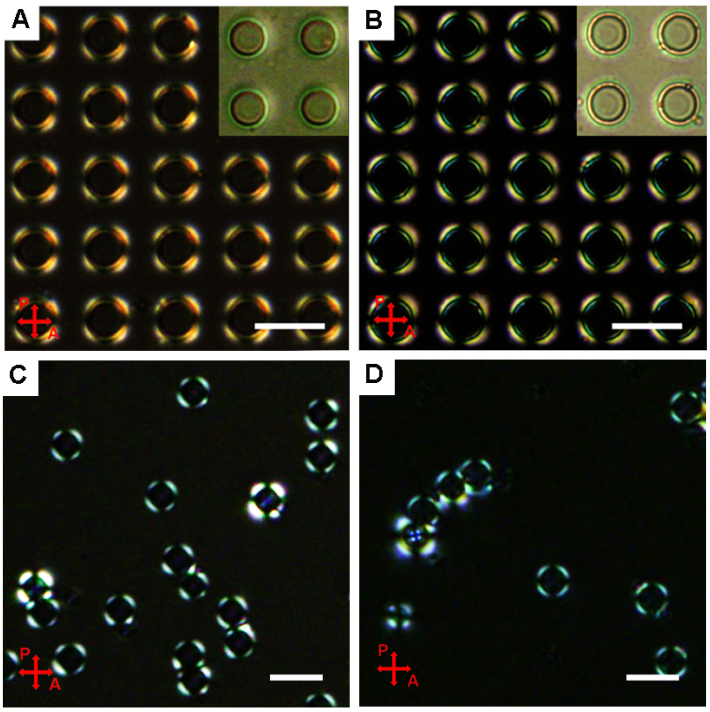

Fig. S7. Maintenance of LC director field during photopolymerization. (A-B) POM and bright field (BF) optical images of LCM_X1 and its polymer in pillar arrays (diameter: 10 µm, pitch: 20 µm, height: 9 µm) with homeotropic anchoring imposed at all surfaces before (A) and after (B) UV curing. Insets in A&B: BF images show possible bulk line defects. (C-D) POM images of silica colloids dispersed in LCM_X1 with homeotropic anchoring at all surfaces before (C) and after (D) UV curing. Scale bars: A-B, 20 µm; C-D, 10 µm.

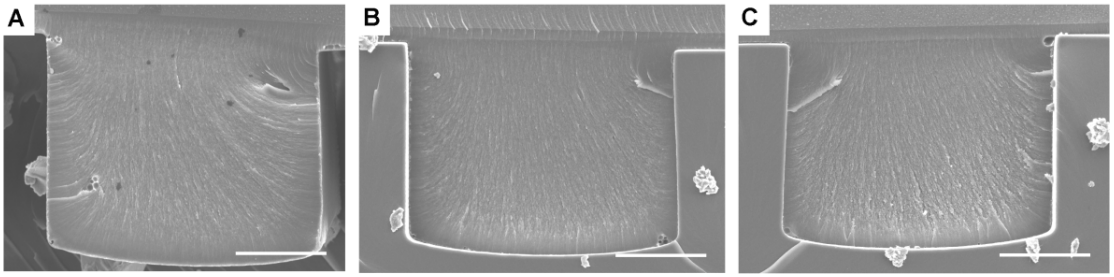

Fig. S8. SEM images of LCP in a channel. Images were taken from three different positions in the sample. Scale bars: 10µm.

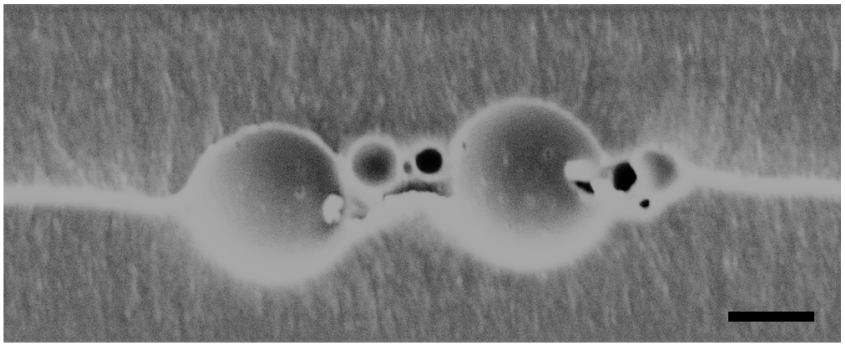

Fig. S9. Merging of the line defects. SEM image of bulk disclination stabilized by multiple colloids. Scale bar: 2 μm

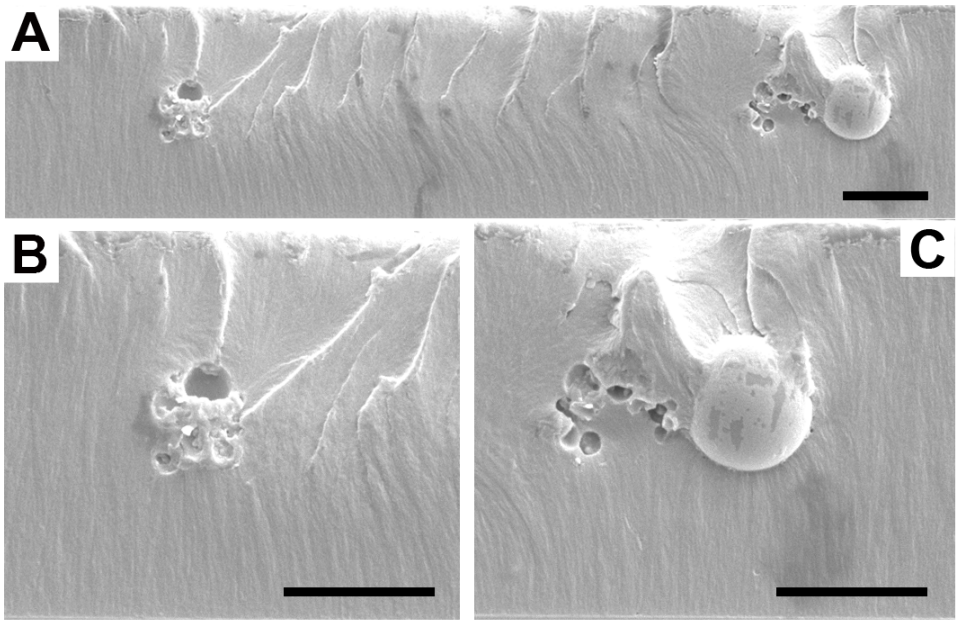

Fig. S10. Escaping behavior of LCs in a planar-like region. SEM images of LCP inside a planar-like region in a homeotropic LC cell. (A) The fracture structure shows stabilization of disclination lines with silica colloids sitting at the two ends of the planar-like region, and the escaping behavior of LC director from right to left. (B-C) A close look at the director field surrounding the colloid. Scale bars: 5 μm

Estimation of the LC elastic constants

As a proof-of-concept, the elastic anisotropy of LCM was estimated by looking at the SEM images (see Fig. S11) of the LCs homeotropically anchored on the walls of a cylindrical pore. The director here "escapes in the third dimension" through a splay/bend deformation. We look at the angle ϑ, that the nematic director adopts at any point relative to the axis of the pore (see Fig. S11 inset), as a function of the radius r, which goes from the center of the pore to its walls. The results are plotted in Fig. S11. We find that the data points can be very satisfactorily fit by(2)

$$\vartheta(r) = 2\tan^{-1}(\alpha\, r/R_0) \qquad (1)$$

where R_0 is the width over which the escape takes place (the radius of the pore), and α is a parameter that depends on the anchoring angle of the director on the homeotropic wall. Specifically, α is equal to the cotangent of the anchoring angle φ_h at the homeotropic wall of the capillary divided by two. Eq. 1 is the theoretical prediction for the escape configuration in a cylindrical channel in the approximation of single elastic constant. It holds when the splay constant and the bend constant are equal.

There is no *a priori* reason why this should be true for our monomers. However, Fig. S11 shows a good agreement between the experimental data and the theoretical prediction, which suggests that the ratio between splay and bend constant for our monomers is close to one. As shown in the literature(3), elastic anisotropy would lead to deviations from this curve.

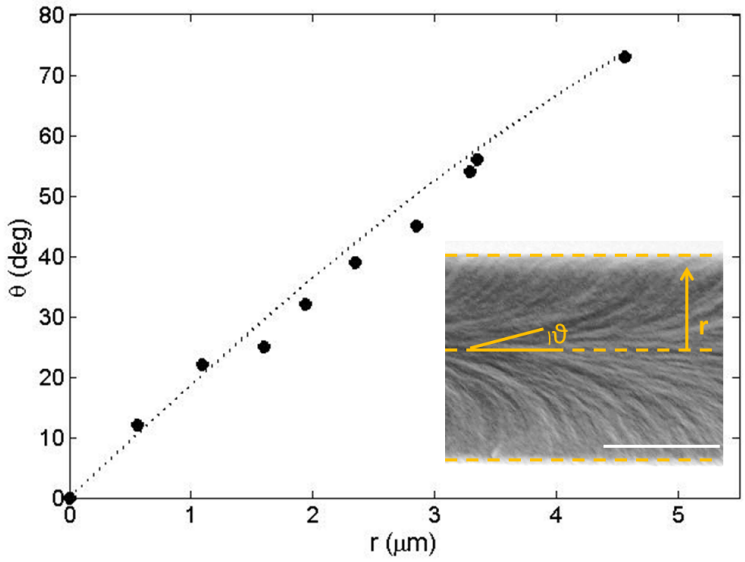

Fig. S11. Director angle as a function of the radial coordinate r. The points are calculated from the escape configuration shown in the inset (scale bar, 5 μm). The line is calculated from Eq. 1.

We do not get information about the twist elastic constant in this configuration, but the lack of twisted escape configuration (observed, for example, in phases with very low twist elastic constant), combined with the observed structure of the hedgehogs near

colloids, suggests that the twist elastic constant is of the same order of magnitude as the other two.

From Eq. 1 and the model proposed by Crawford *et al*. (2), we can also estimate the extrapolation length for homeotropic anchoring, *i.e*. the ratio between the elastic and the anchoring constant. The anchoring angle φ_h on the homeotropic wall is $\varphi_h = \sin^{-1}(((R_0 W_h + K_{24})/K - 1)^{-1})$, where W_h is the homeotropic anchoring constant, K is the elastic constant (always in the one elastic constant approximation), and K_{24} is the saddle-splay constant. If we make the common approximation of neglecting K_{24}, we obtain the extrapolation length $\xi_h = K/W_h = 1.3\mu$.

In order to estimate the extrapolation length in the case of weak planar anchoring, we use a hybrid wedge cell, with one glass untreated (for homeotropic anchoring) and the other one treated with rubbed polyimide. Following the method in the literature (4), we can estimate the extrapolation length by directly measuring the angles formed by the liquid crystals in a hybrid wedge cell with the homeotropic and the planar surfaces, and relating them as:

$$2\,\xi_h(\varphi_p - \varphi_h) = d\sin(2(\Phi_h - \varphi_h)) \quad (2)$$

$$2\,\xi_p(\varphi_p - \varphi_h) = d\sin\left(2(\Phi_p - \varphi_p)\right) \quad (3)$$

Here, the subscript p and h represent the planar and the homeotropic surfaces, respectively, d is the cell thickness, ξ the extrapolation length, Φ the preferred angle with respect to the normal and the flat surface (that is, Φ_h is zero and Φ_p is $\pi/2$), φ is the angle that the nematic director forms with the normal to the cell surface (see Fig. S12). In writing this formula from ref. (4), we already make the approximation that the ratio of the splay and bend elastic constant is close to unity. The extrapolation length can then be estimated at various thicknesses of the wedge cell. We could estimate ξ_h from the study of LCM in the pores with homeotropic anchoring, and that with planar anchoring, ξ_p.

The preferred tilt angle on the planar polyimide surface could be independently estimated by measuring it directly from the SEM images on a planar cell. The points in the SEM image shown in Fig. S12 represent measurements of the extrapolation length at different thickness of the wedge cell, ranging from 6 μ to 30 μm, which gives a value of the planar extrapolation length ~ 10 μm, *i.e*. ten times longer than the homeotropic extrapolation length. This clearly shows that the anchoring is weaker on the polyimide than on the silica surface.

We should remark that the direct visualization of the director profile by SEM image makes it extremely simple and direct to calculate the relevant parameters for our newly synthesized LC.

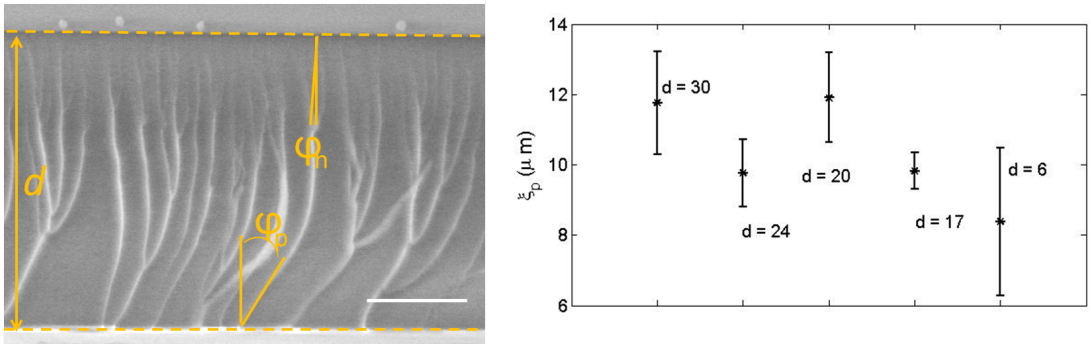

Fig. S12. SEM image of a hybrid wedge cell (left panel), with highlighted angles at the planar and homeotropic surface, and the corresponding measurements of the planar anchoring extrapolation length (right panel) taken from the cell at different cell thicknesses (indicated next to each data point, in microns). Scale bar in SEM image, 10 μm.

A crude estimate of the elastic constants can be obtained simply by dividing the energy necessary to align the mesogens (*i.e.* the thermal energy at the temperature at which the mesogen achieves its alignment, around 370K) by the molecular size *a*.
$K = k_B T/a$ = 1.4*10^{-23} *370 K*0.5*10^{9} m^{-1} = 2.6*10^{-12} N.

Consequently, the homeotropic anchoring constants can be calculated as the ratio between the elastic constant and the extrapolation length: W_h = 2.6*10^{-12} N / 1.3 μm=2*10^{-5} N/m and W_p= 2.6*10^{-6} N/m.

Video S1 shows flow of LCM_X1 between micropillars in real time. One of the cover glasses was patterned with epoxy pillar arrays (D =10 μm, P =20 μm, H=9 μm) coated with silica to impose homeotropic anchoring on all boundaries. The temperature was kept at 90 ^{o}C. The flow was manually created by mechanically pressing the LC sample with tweezers.

Reference:

1. Warenghem, M., "A Test for Surface Energy Anisotropy Sign Determination". *Mol. Cryst. Liq. Cryst.* **1982,** 89 (1-4), 15-21.
2. Crawford, G. P.; Allender, D. W.; Doane, J. W., "Surface elastic and molecular-anchoring properties of nematic liquid crystals confined to cylindrical cavities". *Phys. Rev. A* **1992,** 45 (12), 8693-8708.
3. Scharkowski, A.; Crawford, G. P.; Žumer, S.; Doane, J. W., "A method for the determination of the elastic constant ratio K33/K11 in nematic liquid crystals". *J. Appl. Phys.* **1993,** 73 (11), 7280-7287.
4. Barbero, G.; Madhusudana, N. V.; Durand, G., "Weak anchoring energy and pretilt of a nematic liquid crystal". *J. Phys. Lett.* **1984,** 45 (12), 613-619.